Chapter 4

Active Anticorrosive Coatings for Aluminum Alloys using Adduct Modified Clay Dispersed Polystyrene Nanocomposites

4.1. ABSTRACT

The present investigation is on processing of a series of polystyrene clay nanocomposite (PSC) coatings containing different adduct modified clay (AMC) for corrosion resistance coating applications. The corrosion properties were studied using potentiodynamic and electrochemical impedance spectroscopy measurements in 3.5 wt.% aqueous NaCl electrolyte. The PSC coatings offered enhanced corrosion protection for Aluminum 6061 alloy even at high clay loading (20 wt.%). The order of their protection efficiency was PSC-AMC> Pristine PS > Pristine Na^+-MMT.

4.2. INTRODUCTION

Corrosion of metal is one of the major issues faced by several industries worldwide and different types of coatings are used to control it. Nowadays corrosion control strategies are becoming a challenging task for the material scientists for the use of the materials in extensive environments with multifunctional requirements. A considerable number of coating materials were reported for corrosion protection of the metal surface. Chromate conversion coatings were considered to be an effective corrosion inhibitor for Aluminum alloy (Clark et al., 2002; He et al., 2000). However,

cancerogenic chromate coatings are currently banned due to the adverse environmental and health concern. Later, various non-chromate "green alternatives" coatings, organic or polymeric coating materials and superhydrophobic films were developed as protective coatings for corrosion protection (Abdullayev et al., 2013; Borisova et al., 2012; Chang et al., 2013; Chen et al., 2011; de Leon et al., 2012; Faure et al., 2011; Ghazi et al., 2015; Guo et al., 2009). But small defects in the neat polymeric coatings can provide pathways for corrosive species to penetrate and results in localized corrosion to the metallic substrate. Now as an alternative, various nanoscale inorganic fillers were added to the polymer matrix to generate a series of organic-inorganic hybrid corrosion protection coatings.

The incorporation of the montmorillonite (MMT) into various polymeric matrixes effectively enhanced the corrosion protection effect of pristine polymer (e.g.polyaniline, polymethylmethacrylate, polystyrene (Yeh et al., 2001, 2004c,b)). Exfoliation or complete dispersion of clay layers into individual clay platelets within the polymer matrix leads to significant improvements in physical and chemical properties such as thermal (Lan et al., 1994; Messersmith and Giannelis, 1994; Tyan et al., 1999), mechanical (Shi et al.,1996), gas barrier (Messersmith, and Giannelis, et al.,1995), flame-retardant (Gilman 1999; Gilman et al., 2000; Porter et al., 2000), solvent resistance (Burnside and Giannelis, et al.,1995), and electrorheology properties (Kim et al., 2001). Heinz has reviewed the surface modification of clay minerals and its application in the synthesis of nanocomposites (Heinz, 2012). MMT clay has drawn considerable research

interest due to its lamellar display, high in-plane strength, stiffness and high aspect ratio. Exfoliation behaviour of polymer clay nanocomposite have been investigated using different alkylammonium modified clay (Fu and Heinz, 2010). Yeh et al. (2004a, 2007) has reported that the incorporation of various polymers into the interlayer spaces of organophilic clay can effectively enhance the corrosion protection of polymer over metallic surfaces. Corrosion protection efficiency of polymer clay nanocomposite (PCN) coatings performed at different measured temperature was reported by Chang et al. (2008). Here the dispersion of the clay layers in the polymer matrix increases the length of diffusion pathway for O_2 and H^+. However, the corrosion protection effect of clay polystyrene nanocomposite coatings (PSC) using adduct modified clay on Aluminum 6061 alloy (Al alloy) has never been reported.

Therefore, the present paper highlights on the synthesis and detailed investigation of corrosion resistance performance of different adduct modified clay PSC coatings over pristine polystyrene using a series of electrochemical and impedance measurements. Corrosion protection studies were performed on sample-coated Al alloy immersed in 3.5 wt.% aqueous NaCl electrolyte. Advantages of this method include (i) exfoliated composite coatings showing efficient corrosion resistance properties even at high clay loading (20 wt.%) were obtained (ii) layer by layer self-assembly of clay platelets provide significant increase in barrier properties and (iii) a much simpler step was adopted for the clay modify cation using adducts

instead of commonly used quaternary ammonium salt as intercalating agent.

4.3. EXPERIMENTAL

4.3.1. Materials

Styrene monomer (99%), Oleic acid (OA), Acrylic acid (AA), Cinnamic acid (CC) and CetylTrimethyl Ammonium Bromide (CTAB) was purchased from Sigma-Aldrich Chemicals, USA. Sodium montmorillonite (Na^+-MMT) was obtained from Southern Clay Products, USA with a cation exchange capacity (CEC) of 92.6 meq/ 100g clay. The initiator Benzoyl peroxide (BPO) from SD Fine Chemical Ltd., India was recrystallized from ethanol. Ethanol, Methanol, N-Methyl pyrrolidone (NMP), Toluene and Tetrahydrofuran (THF) of HPLC grade were obtained were obtained from Merck Specialties Pvt. Ltd., India. Aluminum 6061 wrought alloy of composition Al-1.5Mg-0.6Si were used as the coating substrates.

4.3.2. Methods

Polystyrene clay nanocomposite was synthesized by in-situ polymerization of styrene using Adduct modified clay. The organomodified clays were obtained via cation exchange of Na^+ with adducts. Adducts were prepared by treating equimolar concentration of Cetyltrimethylammonium bromide (CTAB) with unsaturated organic acids like Acrylic acid (AA), Cinnamic acid (CA) and Oleic acid (OA). The hydroxyl group of the acid react with CTAB to form an adduct, were as olefinic part of the acid is used

for the polymerization reaction. 1 g of CLAY (cation exchange capacity (CEC) = 92.6 meq/100g) was dispersed in 200 mL of distilled water and stirred for 1 h until a homogeneous mixture was formed. Pre-dissolved 1:1 equimolar concentration of the Acrylic acid-CTAB mixture (equivalent to 2 CEC of the clay) was slowly added to the clay suspension and stirred uninterrupted for 48 h. Finally, the organoclay was recovered by ultra-centrifuging and was dried overnight in a vacuum oven at 80°C to obtain Acrylic acid-CTAB Adduct modified clay and was designated as (AC-AMC). The same procedure was used to prepare Cinnamic acid-CTAB and Oleic acid-CTAB modified clay. The resultant clay were identified as (CC-AMC) and (OC-AMC), respectively. For comparison, CTAB modified clay (CTAB-MC) was also prepared using the same procedure.

For composite preparation, AC-AMC loadings were varied from 1-20 wt%. The Styrene monomer (1.1 ml) was charged into a round-bottom flask with the required amount of AC-AMC. The mixture was ultrasonicated for 10 min to ensure proper dispersion of the clay and was degassed with dry nitrogen for about 20 min prior to the addition of BPO initiator (2 wt.%). Polymerization was then carried out at 70°C by keeping in a temperature controlled oil bath under magnetic stirring (~500 rpm) for 3 h and then at 90°C for 10 h. The solid composite synthesized was dispersed in a minimum amount of toluene, centrifuged to remove insoluble or suspended particles, and the soluble fraction was then precipitated in methanol. Finally, the precipitate was filtered and dried at 60°C to obtain the polystyrene clay nanocomposite. The polystyrene

nanocomposite filled with 1, 3, 5, 10 and 20 wt.% AC-AMC were labelled as PSC-AC1, PSC-AC3, PSC-AC5, PSC-AC10 and PSC-AC20 respectively. The maximum yield and stable composite coatings were obtained at 10 wt.% clay loading.

Hence, the same procedure was followed for the preparation of 10 wt.% PSC using (CC-AMC) and (OC-AMC), and the as-synthesized composites were labelled as (PSC-CC10) and (PSC-OC10), respectively. For coating studies, the pristine polystyrene (PS) was synthesized following the same procedure without the addition of clay.

4.3.3. Characterization Techniques

The functional group characterization of modified clays was carried out using FT-IR spectroscopy with a fully computerized Nicolet Impact 400D FT-IR spectrophotometer. Samples were mixed thoroughly with potassium bromide and compressed into pellets before recording. All spectra were corrected for the presence of moisture and carbon dioxide in the optical path. The extent of intercalation and exfoliation of clay and PSC were characterized using WAXS and SAXS, respectively. WAXS and SAXS analysis were conducted on an XEUSS 2D SAXS/WAXS system using a Genix micro source from Xenocs operated at 50 KV and 0.3 mA. The Cu-Kα radiation (λ=1.54 Å) was collimated with an FOX2D mirror and two pairs of scatter less slits from Xenocs. The d-spacing of the materials were calculated from the angular position 2θ of the observed d_{hkl} reflection peaks based on the Bragg's formula $n\lambda = 2d\sin\theta$, where λ is the wavelength of the X-ray beam and θ is the diffraction angle. Thermal

stability measurements were performed at a heating rate of 10°C/min in a nitrogen atmosphere using Shimadzu, DTG-60 equipment. Electrical conductivity of pellets were measured using the standard spring loaded pressure contact four-probe method using a Keithley 6881 programmable current source and a 2128 A nano-voltmeter at 30°C supplied by Keithley (Germany) as per the standard procedure ASTM F 43-99. For conductivity measurements, the samples were pressed into a 5 mm diameter disk using a hydraulic press operated at a pressure of 200 MPa. SEM observations were made by subjecting the thin gold-coated samples to a Zeiss EVO 18 cryo SEM working at 20−30 kV. The optical properties of the PSC samples were measured (300-700 nm) with a UV-visible Spectrophotometer (Shimadzu UV-3600 with an integrating sphere attachment, ISR-3100) using barium sulphate as a reference.

Electrochemical corrosion measurements

The electrochemical measurements of coated samples were carried by using an AutoLab (PGSTAT302N) potentiostat/galvanostat at room temperature. A single compartment conventional three electrode cell setup was used throughout the experiments and the electrolyte was NaCl (3.5 wt.%) aqueous solution. The PS and PSC coating were prepared by dissolving 6 wt.% of the PS and PSC fine powder in NMP solvent . Drops of corresponding solutions were subsequently spread onto the Aluminum 6061 alloy coupons and cured in an oven at 40°C for 2 h. Then the coated coupons were allowed to completely dry for 24 h at 100°C. The thickness of the coatings was measured by a digimatic micrometer (Mitutoyo) and the

film thickness of all the coatings was about 20 ± 2 μm.For the electrochemical measurements, coated and uncoated Al alloy coupons (1 x 1 cm working area) were used as working electrodes, platinum foil was the counter electrode and saturated calomel electrode (SCE) was the reference electrode.

The potentiodynamic polarization and electrochemical impedance measurements were recorded with respect to the open circuit potentials (OCP). In order to get the stable OCP, the cell setup was kept at least 20 minutes prior to start the measurements. In the polarization curves, E_{corr}, I_{corr}, R_p, tafel slopes, corrosion rates were obtained by the autolab software. E_{corr} value was obtained by scanning the potential from -500 mV to +500 mV with the scan rate of 5mV/s. In the EIS measurements, R_s, R_p, and R_{ct} values were obtained by Frequency response analyser software (FRS). Frequency range used was 100 KHz to 0.1 Hz. All the electrochemical measurements were replicated at least three times to ensure the reproducibility.

4.4. RESULTS AND DISCUSSION

4.4.1. XRD Analysis

In this study, a series of adducts using equimolar concentration of acid-amine having reactive sites were designed as clay modifiers to investigate the effect of the architecture on the physical properties of the resultant nanocomposites. Extent of the cationic exchange was analyzed by WAXS, and the results were plotted in Figure. 4.1A. The (001) reflection of

all the clay appeared at smaller angles (2θ) as compared to the pristine clay indicating the successful ion exchange. The basal space increased from 1.24 nm (2θ = 7.12°) for pristine clay to a maximum of 2.12 nm (2θ = 4.16°) for AC-AMC. Similarly for CC-AMC and OC-AMC the basal spacing has increased to 2.03 nm (2θ = 4.35°) and 1.96 nm (2θ = 4.5°), respectively. These results reveal that the increase in interlayer space was due to the inclusion of adduct within the interlayer of the clay during the ion-exchange reaction. To compare the intercalation efficiency of Adduct over commonly used CTAB surfactant, the d_{001}-value for CTAB- clay was measured. It showed a basal spacing of 1.75nm (2θ = 5.04°), which is less than all the three AMC. These results, in turn confirms that adducts are better intercalating agent than commonly used quaternary ammonium salt for clay.

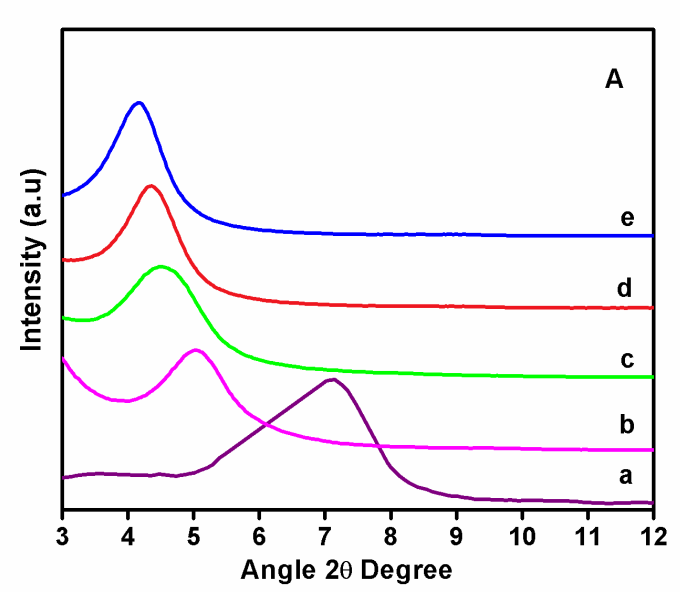

Figure 4.1A. Wide-angle powder X-ray diffraction patterns of (a) Pristine clay, (b) CTAB-MC, (c) OC-AMC, (d) CC-AMC and (e) AC-AMC

It was visually observed that all the clay swelled completely in styrene monomer and caused gelling of the solution upon the sonication. Gelation indicates the clay and styrene are chemically compatible and swelling of clay in monomer indicates the compatibility of the clay with the monomer (Simons et al., 2010). Arioli et al., 2006 reported that higher the swelling the better dispersion of clay in the final composite.

The SAXS patterns of a series of polystyrene clay nanocomposite with three different adducts and also by varying the clay loading of PSC-AC (1, 3, 5, 10 and 20 wt.%) are presented in Figure.4.1B.

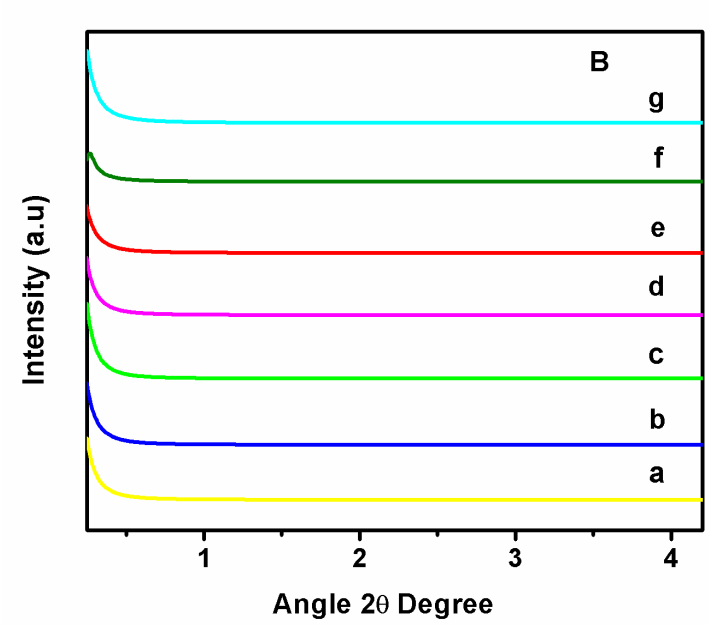

Figureure 4.1B. Small-angle powder X-ray diffraction patterns of (a) PSC-AC1, (b) PSC-AC3, (c) PSC-AC5, (d) PSC-AC10, (e) PSC-OC10, (f) PSC-CC10 and (g) PSC-AC20

Disappearance of (001) reflection peaks for all the PSC indicates the existence of exfoliated structure. The absence of the 001 reflection suggests that the d001-value between the layered silicates is intercalated to spacing

greater than the measurable range, or clay layers are disorderly dispersed in the polystyrene matrix.

4.4.2. FT-IR Spectroscopy

FT-IR spectroscopic studies also support the successful intercalation of adduct into the interlayer space of clay. FT-IR spectra obtained for both Na^+-MMT and AMC are shown in Figure 4.2. In all of the FTIR spectra, the characteristic peaks found at 1028 cm^{-1} and 3445 cm^{-1} were attributed to the Si-O-Si asymmetric stretching of silicate and structural hydroxyls, respectively. In the case of pure clay, the intense characteristic peaks at 2848 and 2926 cm^{-1} were observed due to the stretching vibration for $–CH_2$ and $–CH_3$, respectively. These absorption bands confirm the intercalation of the alkyl group of CTAB in the interlayer of all clay. The characteristic peak at 1642 cm^{-1} was assigned to C=C symmetric stretching of AC-AMC and OC-AMC, and C=C symmetric stretching of aromatic ring of CC-AMC was found at 1635 cm^{-1}. Moreover, characteristic peak at 1692 cm^{-1} was designated as C=O stretching for conjugated and aromatic acid group of AC-AMC and CC-AMC, respectively and characteristic peak found at 1716 cm^{-1} corresponded to the C=O stretching of saturated acid group of OC-AMC. The changes in the characteristic peaks of the spectra for adduct modified clay indicate that the pristine clay was almost entirely converted into the corresponding adduct modified clay.

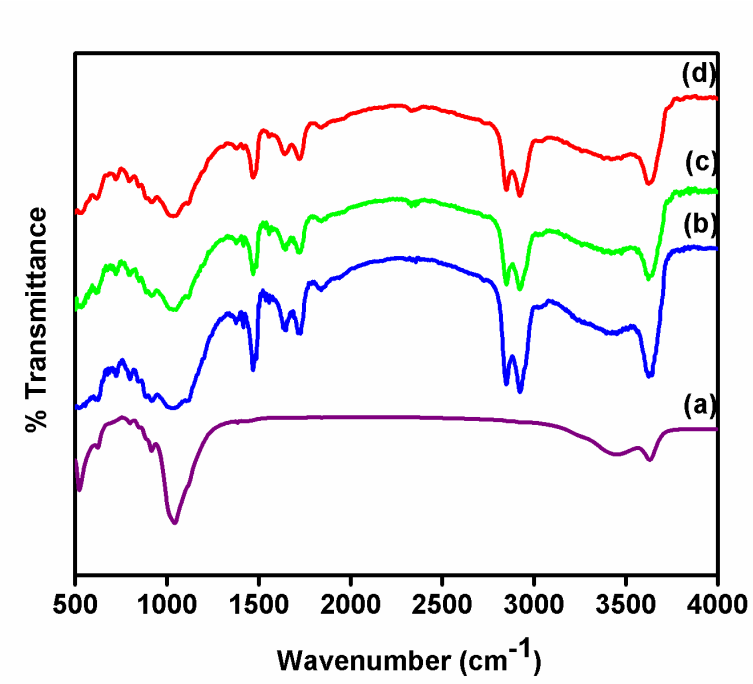

Figure 4.2. FTIR spectra of (a) Pristine clay (b) AC-AMC, (c) OC-AMC, and (d) CC-AMC.

4.4.3. Potentiodynamic Measurements

Quantitative measurement of corrosion protection efficiency of the coatings was performed by potentiodynamic polarization measurement (i.e., corrosion potential (E_{corr}), polarization resistance (R_p), corrosion current (I_{corr}), and corrosion rate (R_{corr}) in a corrosive medium (3.5 wt.% NaCl electrolyte)). In general, higher E_{corr} and R_p and a lower I_{corr} and R_{corr} value indicate the enhanced corrosion protection. SEM images of the polished Al alloy and PSC-coated Al alloy were shown in Figure 4.3.

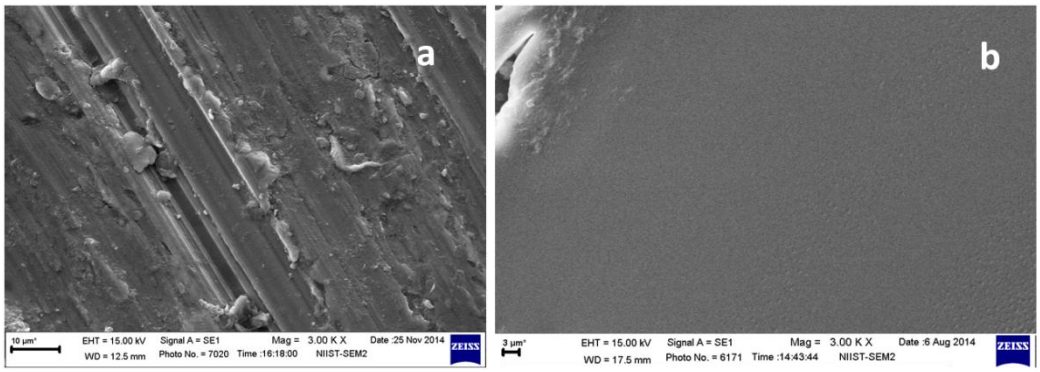

Figure 4.3. SEM micrographs of (a) Polished Al alloy and (b) PSC-AC10 coated Al alloy

Tafel plots and the calculated Tafel parameters for uncoated, PS-coated, and PSC-coated Al alloy samples were shown in Figure 4.4A and 4.4B and corresponding data are listed in Table 4.1. The corrosion protection efficiency increases with positive shift in E_{corr} value. Corrosion potential, E_{corr} value obtained for PS-coated Al alloy electrodes (-845 mV) was more positive than that for the bare Al alloy -952 mV. Moreover, the PSC-coated Al alloy electrodes exhibited a higher positive shift in E_{corr} value than that of PS-coated electrode. This positive shift in E_{corr} shows the protection efficiency of PSC-coatings on Al alloy. Between the three different adduct modified composites the PSC-AC10 (-588 mV vs. SCE) coated electrode showed more positive shift than that of PSC-CC10 (-623 mV vs. SCE) and PSC- OC10 (-648 mV vs. SCE) coated Al alloy electrodes. Moreover, corrosion protection efficiency was significantly improved by increasing the clay loading (i.e., 1 - 20 wt.%). For example, E_{corr} increased from -719 mV for PSC-AC1 to -509 mV for PSC-AC20-coated Al alloy. The PSC-AC20 coatings were found to be less stable as it peels off slowly from Al alloy surface due to its brittle nature that is

attributed to the presence of higher clay content in the composite. Therefore, the PSC-AC10 coating with E_{corr} value -588 mV is more stable and noble towards the electrochemical corrosion. The measured corrosion current (I_{corr}) for PSC-AC10 (0.47 μA/cm^2) coated Al alloy electrode is lower than the corrosion current for uncoated (10.51 μA/cm^2) and PS-coated (4.30 μA/cm$^{2)}$ Al alloy and corresponded to a corrosion rate (R_{corr}) of about 0.16 MPY. Polarization resistance (R_p) value 158 kΩcm^2 in 3.5 wt.%NaCl approaches three times higher order of magnitude greater than uncoated Al alloy. Therefore, on the basis of electrochemical measurements the PSC-AC10-coated Al alloy strips resists corrosion better than the uncoated and PS-coated Al alloy electrodes.

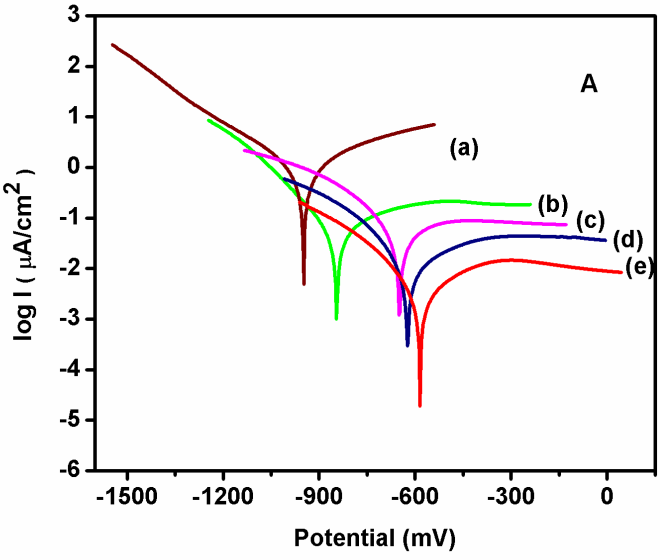

Figure.4.4A. Tafel plots for (a) uncoated (b) PS-coated, (c) PSC-OC10-coated, (d) PSC-CC10-coated and (e) PSC-AC10 coated Al alloy measured in 3.5 wt.% aqueous NaCl solution

Table 4.1. Electrochemical corrosion measurements of Bare, PS-coated, and PSC-coated Al-Alloy

Sample Code	Feed composition (wt %)		Electrochemical corrosion measurement			
	PS	MMT	E_{corr} (mV)	R_p ($k\Omega cm^2$)	I_{corr} ($\mu A/cm^2$)	R_{corr} (*MPY*))
Bare	-	-	-952	0.46	10.51	8.36
PS	100	-	-845	2.14	4.30	1.93
PSC-AC1	99.00	1.00	-719	8.56	2.76	1.03
PSC-AC3	97.00	3.00	-695	21.92	1.25	0.86
PSC-AC5	95.00	5.00	-648	53.83	0.92	0.57
PSC-AC10	90.00	10.00	-588	158.00	0.47	0.16
PSC-AC20	80.00	20.00	-509	196.55	0.24	0.03
PSC-CC10	90.00	10.00	-623	112.48	0.51	0.22
PSC-OC10	90.00	10.00	-648	125.77	0.55	0.27

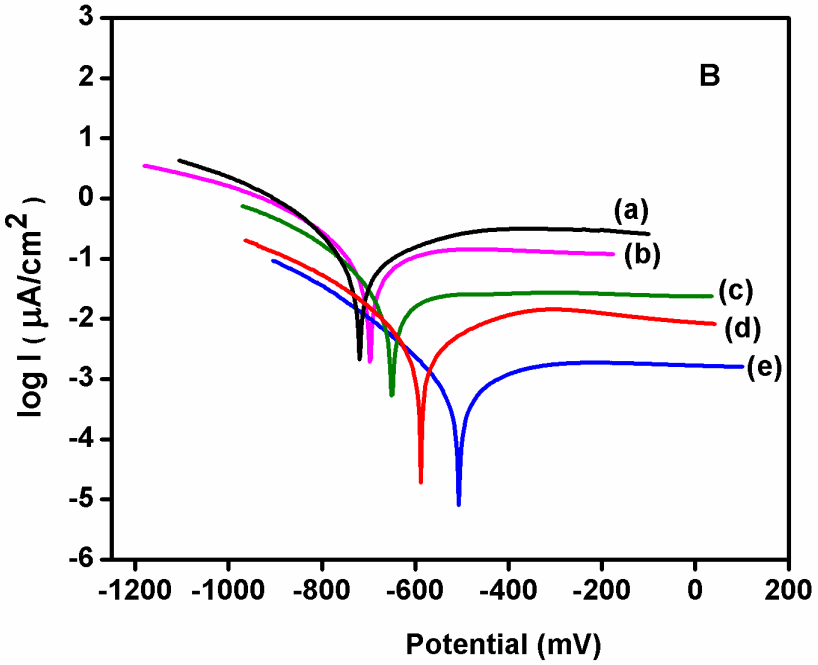

Figure.4.4B. Tafel plots for (a) PSC-AC1-coated, (b) PSC-AC3-coated, (c) PSC-AC5-coated and (d) PSC-AC20-coated Al alloy measured in 3.5 wt.% NaCl aqueous solution

The enhanced corrosion protection of AMC dispersed polystyrene nanocomposites is due to the increased clay loading and the nature of adduct, indicating that the organophilic clay with a plate-like shape increases the length of the diffusion pathways for attacking species.

4.4.4. Electrochemical Impedance measurement

Electrochemical impedance spectroscopy (EIS) was used to determine the corrosion activity difference between the surface of uncoated and PS and PSC-coated Al alloy. Impedance is a complex resistance when a current flow through a circuit made of capacitors, resistors, or insulators, or any combination out of that (Park and Yoo, 2003). EIS measurements result in currents produced over a wide range of frequencies. For simulation studies, corrosive metals are modelled using an equivalent circuit called a Randles circuit. As shown in Figure. 4.5., it consists of a double-layer capacitor connected in parallel with a charge-transfer resistor and in series with an electrolyte solution resistor. The impedance (Z) depends on the charge transfer resistance (R_{ct}), the solution resistance (R_s), the capacitance of the electrical double layer, and the frequency of the AC signal (ω). Z can be deduced as follows:

$$Z = Z' + jZ'' \quad .....(1)$$

$$= R_s + R_{ct} / [1 + (R_{ct}C_{dl}\omega)^2] + j(R^2_{ct}C_{dl}\omega) / [1+ (R_{ct}C_{dl}\omega)^2] \quad .....(2)$$

The high-frequency intercept represents the solution resistance, and the low-frequency intercept represents the sum of the solution and charge transfer resistances. Larger the diameter of the semicircle (charge transfer resistance) lower is the corrosion rate.

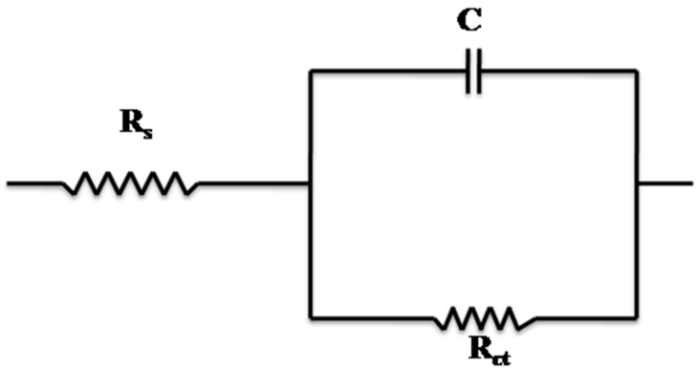

Figure 4.5. Randle circuit

The Nyquist plots measured for six samples of uncoated and coated Al alloy immersed in 3.5 wt.%NaCl aqueous electrolytes are shown in Figure. 4.6. The charge transfer resistances (R_{ct}) of the bare, PS-coated, PSC-AC1-coated, PSC-AC3-coated, PSC-AC5-coated and PSC-AC10-coated electrodes were 0.4, 1.1, 2.3, 3.4, 4.7, and 7.1 $k\Omega.cm^2$, respectively. Coatings with high R_{ct} value offer high corrosion protection. Therefore, from the results it's clear that the PSC-AC10 coatings showed higher R_{ct} value and could offer more effective corrosion protection. This novel property of enhanced anticorrosion effect of PSC materials can be attributed to the effective dispersion of clay platelets in the PS matrix, which in turn increase the tortuosity of the diffusion pathway of attacking species.

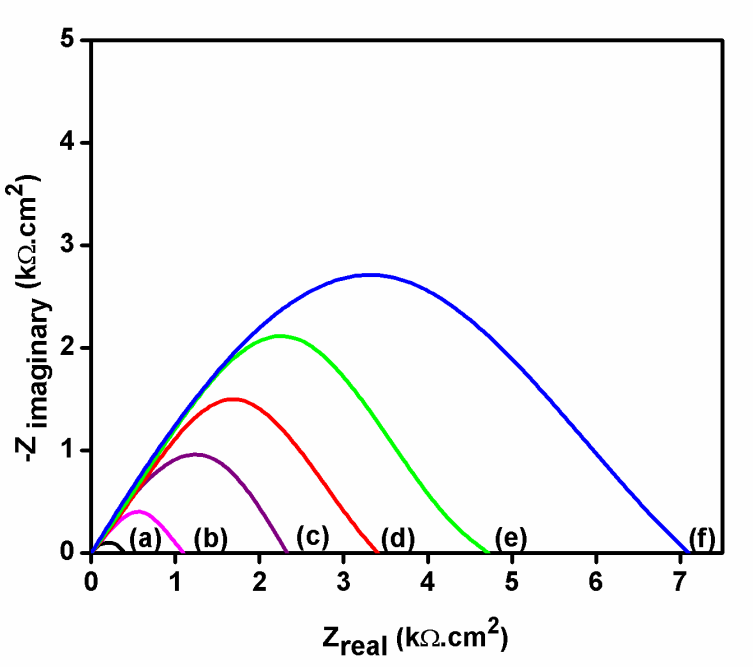

Figure 4.6. Nyquist plots for (a) uncoated, (b) PS-coated (c) PSC-AC1-coated (d) PSC-AC3-coated (e) PSC-AC5-coated and (f) PSC-AC10-coated Al alloy samples immersed in 3.5 wt% NaCl aqueous solution

4.4.5. Thermal Properties of fine powder

TGA has been used extensively to throw light on the precise mode of thermal decomposition behaviour of the PSC. Figure 4.7A and 4.7B are typical thermogram of mass loss as a function of temperature for PS and the PSC materials. In general, there are several stages of weight loss starting from ~250°C and ending at 600°C, which might correspond to the degradation of the intercalating agent followed by the structural decomposition of the polymers. The relative thermal stability of the samples is compared in Table 2 and the onset degradation temperature (T_d - temperature at 10% mass loss) of PSC materials along with pristine PS is given. By the addition of clay, evidently the onset thermal decomposition of

all the PSC materials were shifted significantly towards the higher temperature range than that of pristine PS. After 600°C, all curves became flat and mainly the inorganic residue (i.e., Al_2O_3, MgO, SiO_2) remained.

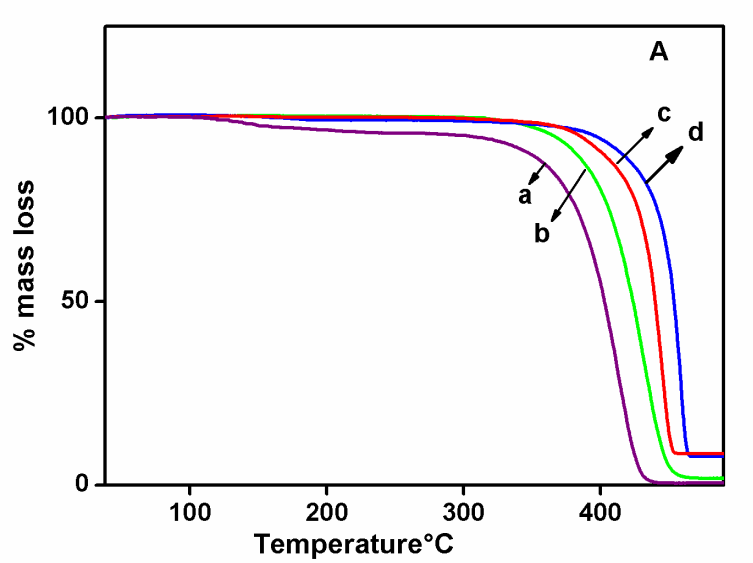

Figure 4.7A. TGA curves of (a) PS, (b) PSC-OC10, (c) PSC-CC10, and (d) PSC-AC10 using different adducts at 10 wt % clay loading

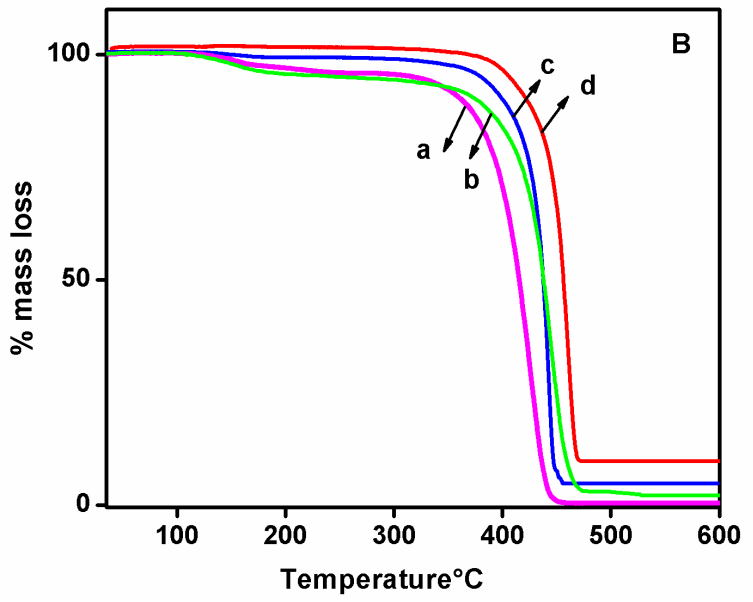

Figure 4.7B. TGA curves of (a) PSC-AC1, (b) PSC-AC3, (c) PSC-AC5, and (d) PSC-AC10 by varying the clay loading (1-10 wt.%)

Thermal phase transition changes (e.g., Glass Transition Temperature T_g) of neat PS and PSC materials were studied by recording DSC at a heating rate of 10°C/min in a nitrogen atmosphere. Figure 4.8A and 4.8B are the DSC scan of the entire sample, in which an endothermic shift in the baseline was observed. The T_g of all the PSC materials was significantly higher than that of pristine PS (Table 4.2). This result indicate that the portion of the intercalated PS chain segments within the interlayer spacing of clay tends to retard the segmental motion of the PS matrix and results in a T_g increase.

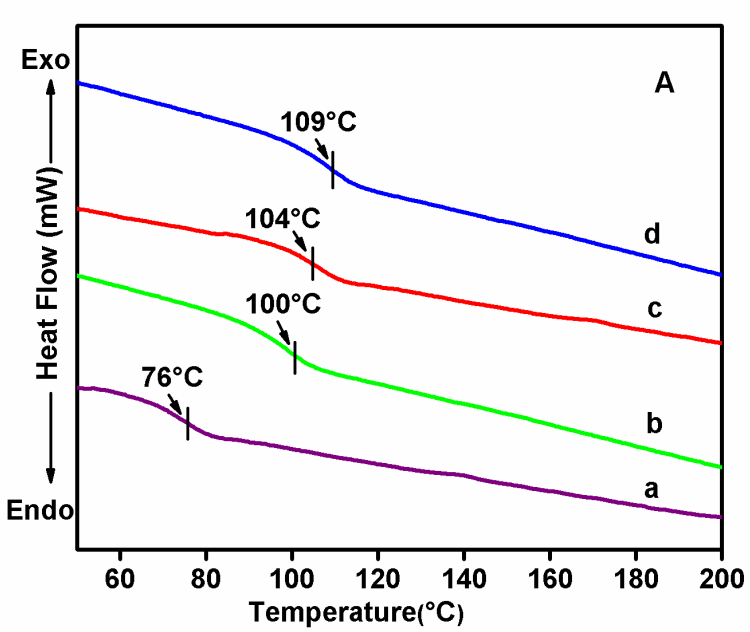

Figure 4.8A. DSC curves of (a) PS, (b) PSC-OC10, (c) PSC-CC10, and (d) PSC-AC10

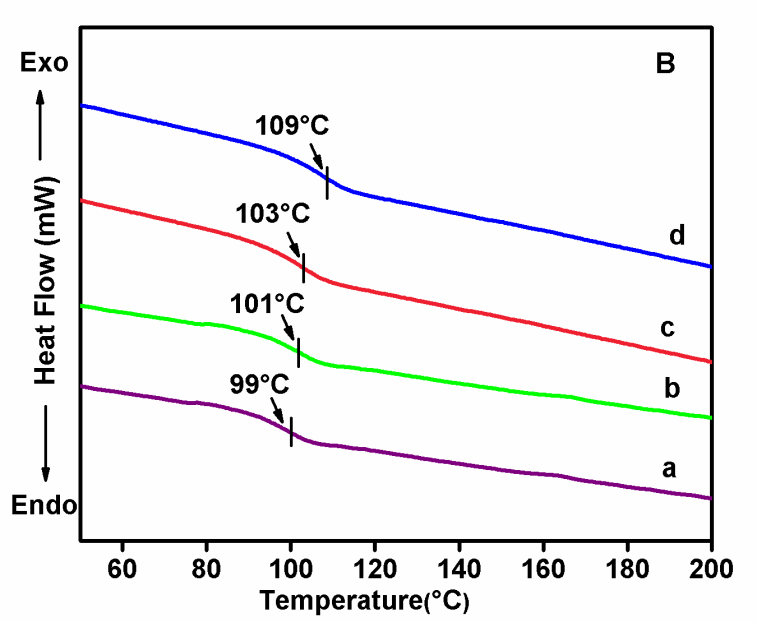

Figure 4.8B. DSC curves of (a) PSC-AC1, (b) PSC-AC3, (c) PSCAC5, and (d) PSC-AC10

Table 4.2. Thermal property and Electrical conductivity measurement of PS and PSC materials

Sample Code	Thermal properties			Electrical Conductivity
	Inorganic content[a] (wt %)	T_d[a] (°C)	T_g[b] (°C)	Conductivity[c] (σ) (S/cm)
PS	-	347	76	19.9×10^{-5}
PSC-AC1	0.5	360	99	14.5×10^{-5}
PSC-AC3	2.1	373	101	13.0×10^{-5}
PSC-AC5	4.0	395	103	12.7×10^{-5}
PSC-AC10	7.5	414	109	11.9×10^{-5}
PSC-CC10	8.4	382	104	-
PSC-OC10	2.3	400	100	-

[a] As determined by thermogravimetric analysis (TGA).
[b] As measured by differential scanning calorimetry (DSC)
[c] As measured by four-point probe technique

4.4.6. Optical Clarity of free-standing film

In this study, the free-standing film of neat PS and PSC-AC materials of ~ 50 μm thickness was used for optical Clarity measurements. It was found that the nanoscale dispersion of the clay in the polystyrene matrix retains its optical clarity even at 5 wt.% clay loading (e.g., PSC-AC5). As observed in Figure. 4.9A the UV-visible transmission spectra of PSC-AC films (1 – 5 wt.%) were almost entirely unaffected by the addition of the clay (in the visible region (400-700 nm) and retained high transparency of PS. Furthermore, it was noted that a further increase of clay loading (10 wt.%) resulted in low transparency of PS matrix.

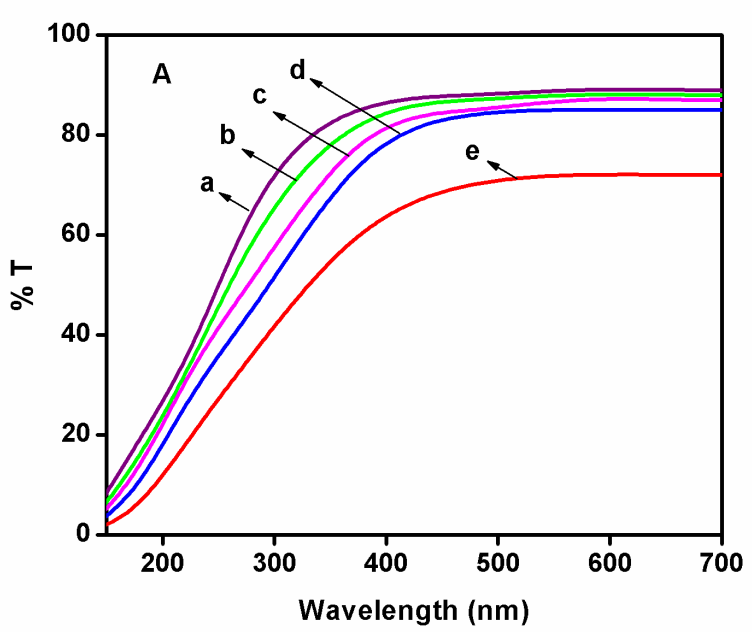

Figure 4.9A. UV-Visible transmission spectra of (a) neat PS, (b) PSC-AC1, (c) PSC-AC3 (d) PSC-AC5 and (e) PSC-AC10

4.4.7. Electrical conductivity of powder pressed pellets

The electrical conductivity of PSC materials along with neat PS measured using four-point probe technique were shown in Figure. 4.9B. The electrical conductivity of PSC-AC (1 - 10 wt.%) were found to be slightly smaller than that of the pristine PS. The results given in Table 4.2 can be attributed to non-electrically conductive Na^{+}-MMT, which is incorporated in the PS matrix of the nanocomposite. This incorporation contributes to a lowering of molecular weight, reflecting a decreased electrical conductivity.

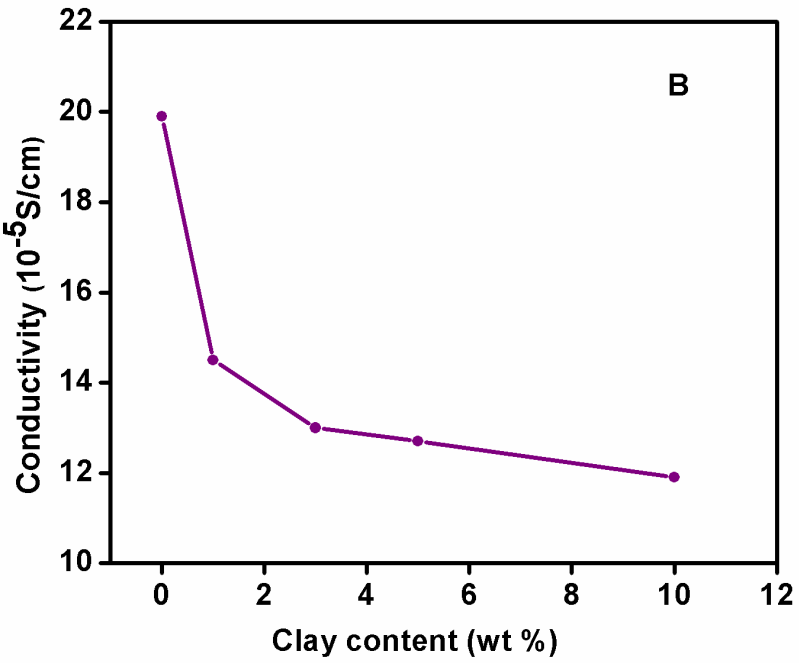

Figure 4.9B. Relationship between electrical conductivity and clay loading as obtained from four-probe technique measurements

4.5. CONCLUSIONS

A series of polystyrene clay nanocompositewere prepared successfully by dispersing the inorganic nanolayers of clay in an organic PS matrix via in situ thermal polymerization. For corrosion studies, electrochemical measurements under 3.5 wt.% NaCl solution were conducted to determine the corrosion protection efficiency of PSC coatings to shield the Aluminum 6061 alloy. The potentiodynamic and electrochemical impedance spectroscopic measurement results showed that the resistance to corrosion of Al alloy was significantly improved by PSC coatings and provided an efficient barrier against aggressive attacking species. The superior anticorrosion property of polystyrene clay nanocomposite materials compared to pristine PS results from dispersing nanolayers of clay in the PS matrix to increase the tortuosity of the diffusion pathway for oxygen and water. The PSC-AC20 coating provided higher protection against corrosion, but due to the high clay content the coating gets peeled off in due course. Comparatively the PSC-AC10 coatings showed better adherence and stability on Al alloys, and it can be easily applied to metal and alloy surfaces for the commercial corrosion resistant application.